Chapter 5

Major Radius Shift Experiment

5.1 Introduction

At first sight, it seems reasonable that as a confined marginally passing α–particle trajectory, such as that shown in Fig. 5.1, moves toward higher magnetic field during an inward major radius shift that the α–particle would mirror and become a trapped particle (shown in Fig. 5.1 by the lighter shade) leading to increased α–particle loss. Increased alpha loss observed using the lost alpha scintillator detectors during previous major radius shifts conducted on TFTR, usually for cross calibration of multi-chord diagnostics, have raised the question whether this alpha loss is induced by the shift itself or by the MHD that is often generated during such shifts. To answer this question, a systematic study of alpha loss during major radius shifts in MHD quiescent plasmas was conducted using the lost alpha scintillator detectors. The alpha collector of Chapters 3 and 4 was not used during this experiment because of the use of large major radius plasmas (R=2.62 m) in which the alpha collector would extend inside the last closed flux surface and overheat. Furthermore, the poor time resolution of the alpha collector makes it unsuited to making observations of a transient nature (e.g. R shifts).

A shift-induced deconfinement of previously confined, marginally passing α–particles to the lost alpha scintillator detectors would make it possible to study the physics of charged particles near the passing/trapped boundary in phase space. In particular, it might be possible to experimentally verify the existence of collisional nonprompt alpha loss (Sec. 2.4.1) [15], which, under steady state conditions, is thought to contribute an insignificant amount (i.e. $< 10\%$) to the total fusion product loss. Fig. 5.2(a) depicts velocity phase space for a fixed r/a outer midplane crossing point of counter-going particles. As α–particles slow down from $v/v_0 = 1$, where v_0 is the birth velocity, they also undergo pitch angle scattering which alters their $v_\perp/v$. This results in the scattering of marginally passing α–particles across the passing/trapped boundary as they slow down, causing these particles to be nonpromptly lost. The passing/trapped boundary moves to higher $v_\perp/v$ at lower v/v_0 due to the improved confinement associated with the narrower banana width at lower energy. Below a certain energy the trapped particles are also confined and no longer contribute to collisional nonprompt

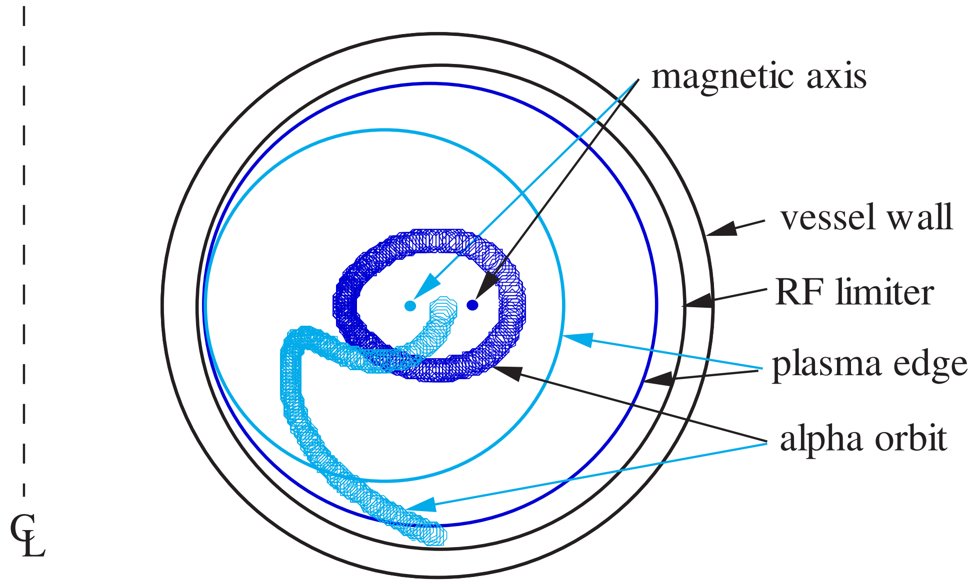

Figure 5.1: *Inward major radius shift of plasma from 2.6 m to 2.4 m (2.4 m features drawn in light shade) causing a marginally passing α–particle orbit to transition to a trapped orbit lost to the 90° detector, assuming no energy is gained by the α–particle during the compression.*

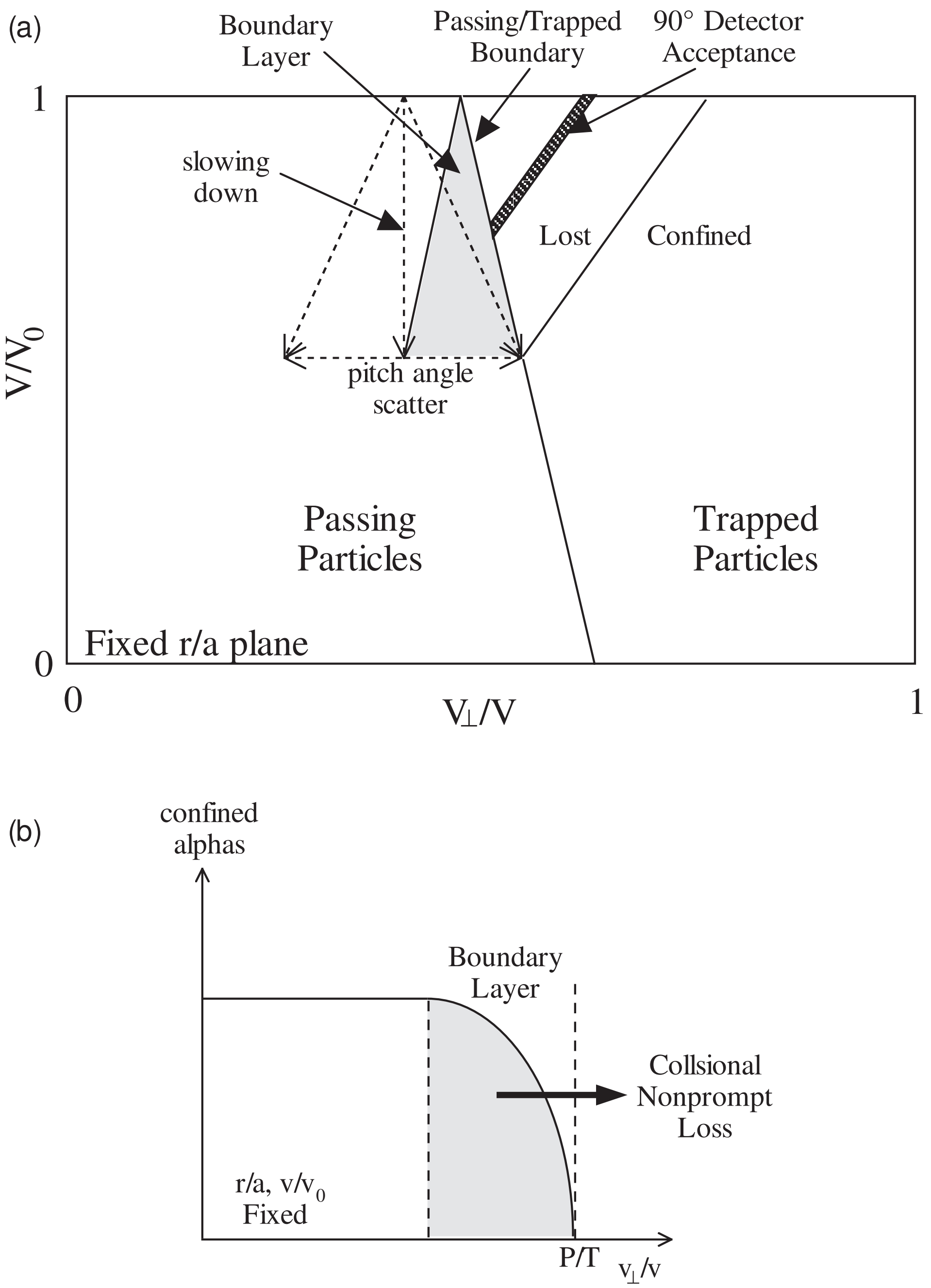

Figure 5.2: *(a) Velocity space depicting slowing down and pitch angle scattering of alphas. Marginally confined passing particles scattering across the passing/trapped boundary create a partially depleted boundary layer as depicted in (b) for fixed r/a and* v/v_0.

loss. The phase space region in which α–particles intercept the 90° detector is also depicted. As shown in Fig. 5.2(b) for a given energy and r/a, this collisional loss process establishes a partially depleted boundary layer near the passing/trapped boundary in which the α–particle distribution function decays to zero at the boundary. The slope of this distribution function should lead to a diffusive flux of particles across the boundary. If an inward major radius shift can cause a shift of the passing/trapped boundary toward the passing region in phase space, however, this loss mechanism can be transiently enhanced by moving the boundary into an undepleted region in phase space.

The inward major radius shift is an adiabatic compression, generated by increasing the vertical magnetic field on a time scale that is slow compared to the thermal particle collision time, but fast compared to the energy confinement time [55]. The toroidal magnetic field is held constant during the shift such that $a \sim R^{1/2}$ to conserve toroidal magnetic flux. At the same time, the plasma current is increased as $I_p \sim R^{-1}$ to maintain the q profile constant. These scalings are modified by the fact that the plasma is continually limited by the bumper limiter at R_{bl} on the high field side. This causes the outer edge of the plasma to be scraped off, since the minor radius is constrained by this limiter to $a = R_0 - R_{bl}$, which decreases faster than $a \sim R^{1/2}$.

During adiabatic compression, the magnetic moment and canonical angular momentum of an α–particle should be conserved. These quantities comprise two of the three constants of the motion needed to fully characterize the guiding-center motion of a charged particle in an axisymmetric tokamak. The third quantity needed to complete the orbit description is the particle's energy. Thus, a determination of the energy gained from compression is required. This energy change can be found by averaging the velocity change along the trajectory of the particle in time [56], and is found to increase in roughly the same proportion as the decrease in plasma major radius for marginally passing α–particles. Somewhat surprisingly, this energy gain is found to be sufficient to allow most marginally passing α–particles to remain passing throughout the major radius shifts such that little or no shift-induced alpha loss is expected.

However, an unexpected loss of partially thermalized alphas lost at the passing/trapped boundary in phase space was observed in this experiment. This anomalous loss occurs at a plasma current of 1.4 MA, but not at 1.0 nor 1.8 MA. It occurs $\sim$ 80 ms after an inward major radius shift from 2.6 to 2.4 m, and persists until the major radius is shifted back out to 2.6 m. Collisional loss and MHD are considered as possible explanations, but neither are consistent with this anomalous loss.

5.2 Experiment

5.2.1 Experimental Design and Initial Expectations

Major radius shifts in TFTR DT discharges were done at three values of plasma current; 1.0, 1.4, and 1.8 MA. All were done at 10 MW of NBI power, low enough to avoid significant MHD activity, but high enough to provide sufficient lost alpha signal. The NBI phase lasted for 1.5 s, as shown in Fig. 5.3(a). The plasma was first allowed to equilibrate for 700 ms after the onset of NBI. The major radius was then shifted inward, as shown in Fig. 5.3(b), from 2.6 m to R' in 80 ms, where R' was 2.4 m for the 1.0 and 1.4 MA discharges, and 2.5 m for the 1.8 MA discharge. The higher current case was more severely limited in shift range by the potential for disruption caused by the edge q passing through a low rational value. The major radius is then shifted back out to 2.6 m, also in 80 ms, starting 320 ms after the end of the first shift. Baseline discharges at 2.6 m and R' were also done at each plasma current for comparison. The TFTR shot numbers for the shifted and baseline (BL) discharges are listed in Table 5.1, along with R' and the value the plasma current was shifted to (I_p') in conjunction with the major radius shift to R'. Each shifted shot was repeated to ensure reproducibility. The backup shot numbers (and corresponding parameters if different from primary shot) are shown in parenthesis. The results presented in the remainder of this chapter are only from the primary shots, but a comparison with the backup shots does show consistency.

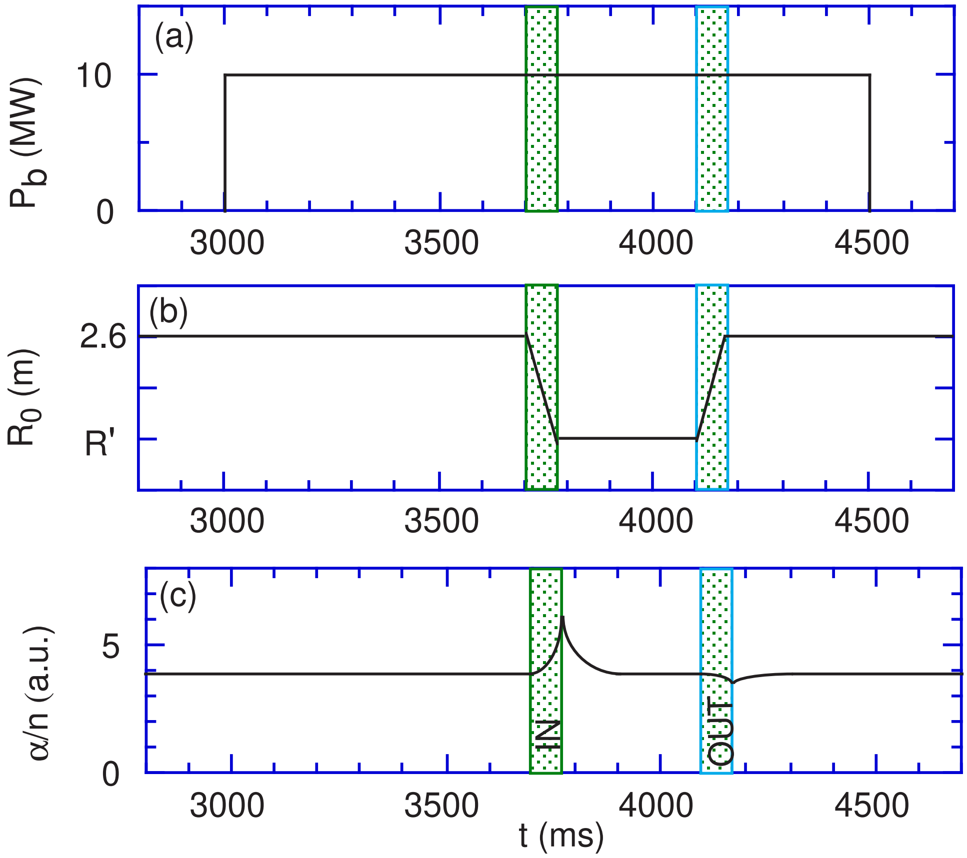

Figure 5.3: *Waveforms for (a) the NBI power, (b) the major radius, and (c) schematic representation of the expected lost–α signal to the* $90°$ *detector.*

The expectation that there would be an increased alpha loss during the IN shift is shown schematically in Fig. 5.3(c). The gradual decay of the peak in the alpha signal was expected with the transient effect of having a more fully populated boundary layer region near the passing/trapped boundary, producing increased collisional non-prompt loss [15] for the length of time it takes to reestablish an equilibrium [57, 58]. It was also expected that an increased alpha loss signal would be accompanied by a widening of the gyroradius distribution and a decrease in the mean gyroradius, since the additional loss would be comprised of α–particles that have been confined long enough to slow down to some degree, and not just birth energy α–particles. Also, because the additional loss should occur at the passing/trapped boundary, the increased loss signal would be accompanied by a narrowing of the pitch angle distribution, since

I_p (MA)	1.0	1.4	1.8
R' (m)	2.4 (2.35)	2.4	2.5
I_p' (MA)	1.1 (1.1)	1.5	1.9
Shifted Shot #	86139 (86171)	86136 (86134)	86144 (86143)
BL Shot # (R_0=2.6 m)	86169	86168	86176
BL Shot # (R_0=R', I_p=I_p')	86167	86166	86175

Table 5.1: *R Shift Shot List*

the additional loss would be more localized in pitch angle than first orbit loss, and a decrease in the mean pitch angle, since the passing/trapped boundary occurs below the mean of the first orbit loss pitch angle distribution.

Little effect was expected during the OUT shift since the passing/trapped boundary was expected to shift in phase space toward a region of trapped particles which had been previously lost on their first orbit (since passing particles are expected to become more passing as the plasma moves to lower magnetic field). A small reduction in the lost alpha signal was, however, expected due to the reduced collisional nonprompt loss associated with the more fully depleted boundary layer region that would be established as a result of the OUT shift.

5.2.2 Experimental Results

Total Alpha flux

Fig. 5.4 shows the neutron normalized 90° lost alpha detector signals as a function of time at the three values of plasma current: (a) 1.0 MA; (b) 1.4 MA; and (c) 1.8 MA. The circle and x symbols correspond to the alpha collection fractions (alphas detected/alphas produced) calculated for first orbit loss by the Lorentz ORBIT code using the alpha source and q radial profiles from TRANSP. The 1.4 MA R shifted

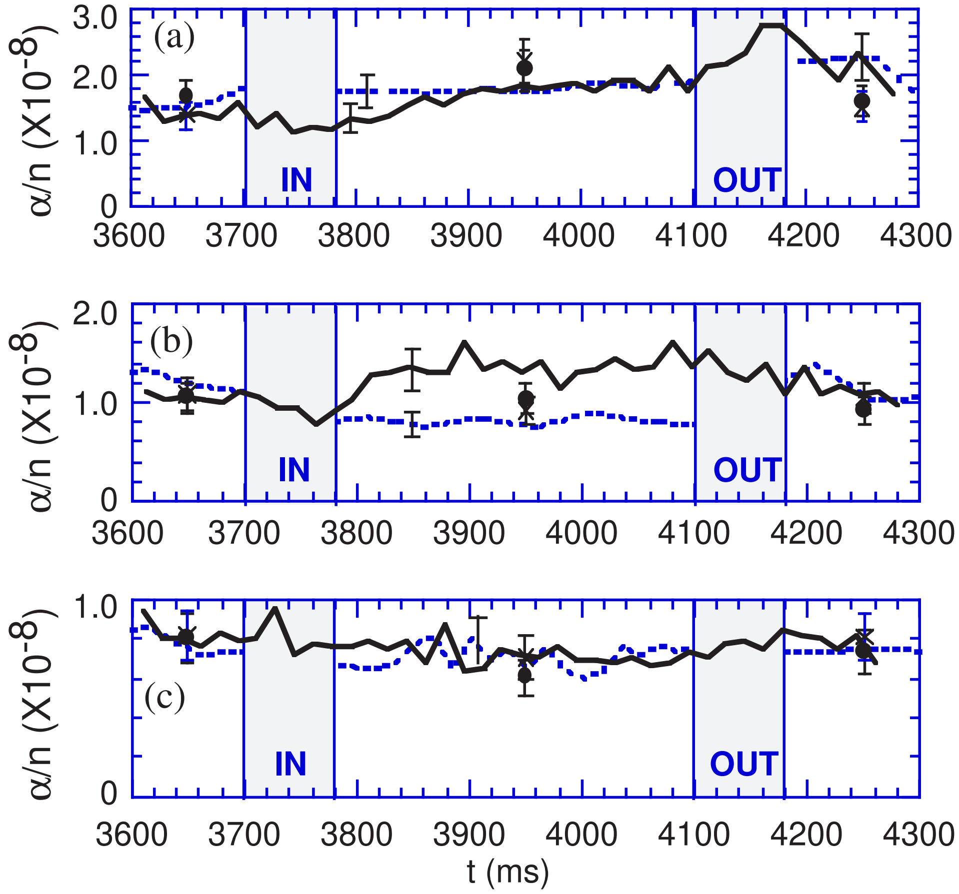

Figure 5.4: 90° *lost alpha detector signals for (a) 1.0 MA, (b) 1.4 MA, and (c) 1.8 MA major radius shifts. Solid traces are for the shifted discharges while the dashed traces are for baseline discharges for comparison. Circle and x symbols correspond to the alpha collection fractions calculated for first orbit loss. Error bars of* ±15% *are based on detector uncertainty.*

signal in Fig. 5.4(b) is normalized to the calculated first orbit alpha collection fraction at 3.65 s. The relative strengths of the remaining signals are preserved such that no further normalizations are needed. For comparison, the signals from two separate baseline discharges at each current, one at 2.6 m (shown before IN and after OUT) and one at R′ (shown between IN and OUT), are shown in dashed lines. The lost alpha signals of the baseline discharges should be comprised predominantly of first orbit loss. With the possible exception of the 1.0 MA discharge in Fig. 5.4(a), there does not appear to be any appreciable change in the alpha signal during the IN shift. The 1.0 MA discharge may be exhibiting a slight decrease in normalized alpha loss during the IN shift, opposite to the expected effect, but the magnitude of this drop is within the uncertainty of the detection method. Similarly, there does not appear to be any significant change during the OUT shift. The most pronounced effect occurs in the 1.4 MA discharge, shown in Fig. 5.4(b), between the IN and OUT shift. Here the shifted discharge displays alpha loss approximately 70% higher than the baseline shot. The first orbit model points for the shifted and baseline shots at 3.95 s, however, do not exhibit this effect. The increased loss takes about 80 ms to build up after the end of the IN shift. This result was unexpected.

Gyroradius Distribution

The 2D images of the scintillator detector are interpreted in terms of gyroradius and pitch angle as discussed in Sec. 2.5.1. Gyroradius distributions are obtained by averaging over a range of pitch angles and vice versa for pitch angle distributions. Fig. 5.5 shows the mean value of the gyroradius distribution (averaged over the full pitch angle range of 40 to 90°) as a function of time for the signals in Fig. 5.4. The mean gyroradii of the shifted discharges agree with that of the baseline shots, within the detector uncertainty, with the exception of the time interval between the IN and OUT shift in the 1.4 MA discharge shown in Fig. 5.5(b). This correlates with the anomalously large signal seen in Fig. 5.4(b). Assuming an anomalous loss flux that is 70% that of first orbit loss, as inferred from Fig. 5.4(b), the decrease in mean gyroradius seen in Fig. 5.5(b) corresponds to an anomalous loss energy of $E_{anom} \approx (0.8 \pm 0.1)E_0$. For the the 1.0 MA discharge shown in Fig. 5.4(a), where

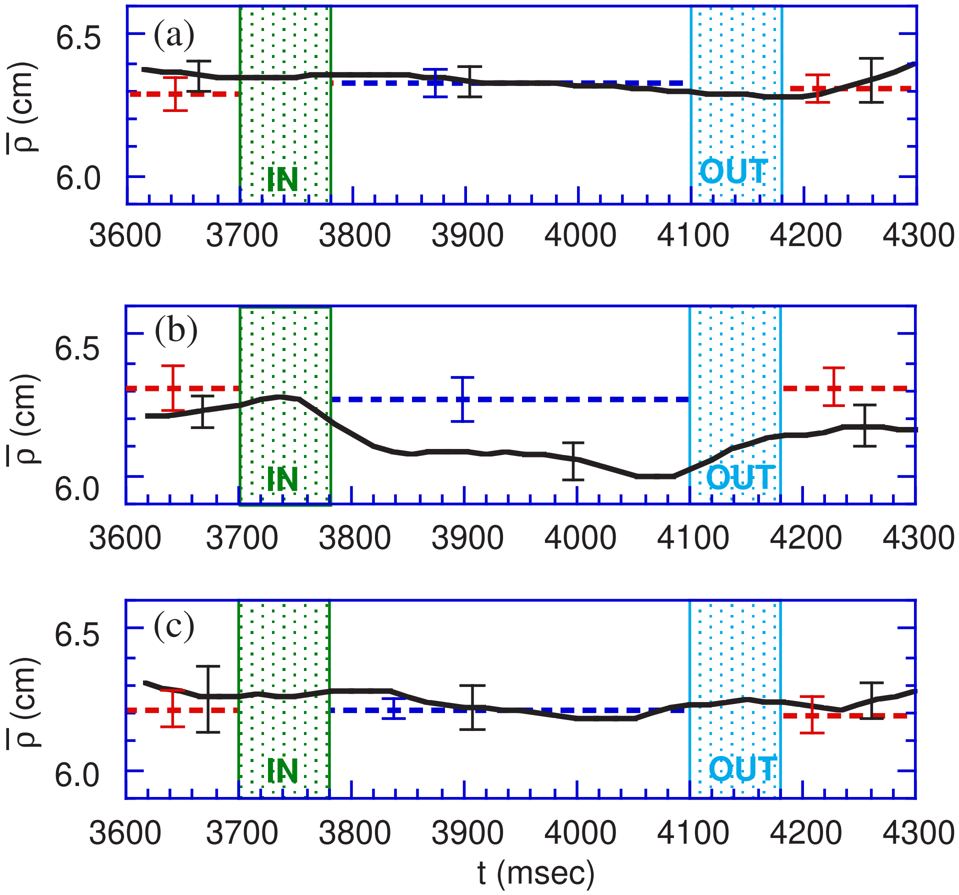

Figure 5.5: *Mean of the gyroradius distribution as a function of time for the* 90° *lost alpha detector signals shown in Fig. 5.4. Error bars based on one standard deviation in data scatter.*

it was not clear if there was an anomalous loss feature, there does not appear to be any significant deviation from the baseline mean gyroradius during the IN and OUT shifts, making it consistent with first orbit loss at 3.5 MeV.

Pitch Angle Distribution

Fig. 5.6 shows the mean value of the pitch angle distribution as a function of time for the signals in Fig. 5.4. The mean pitch angles of the shifted discharges agree with that of the baseline shots for each of the plasma currents, within the detector uncertainty,

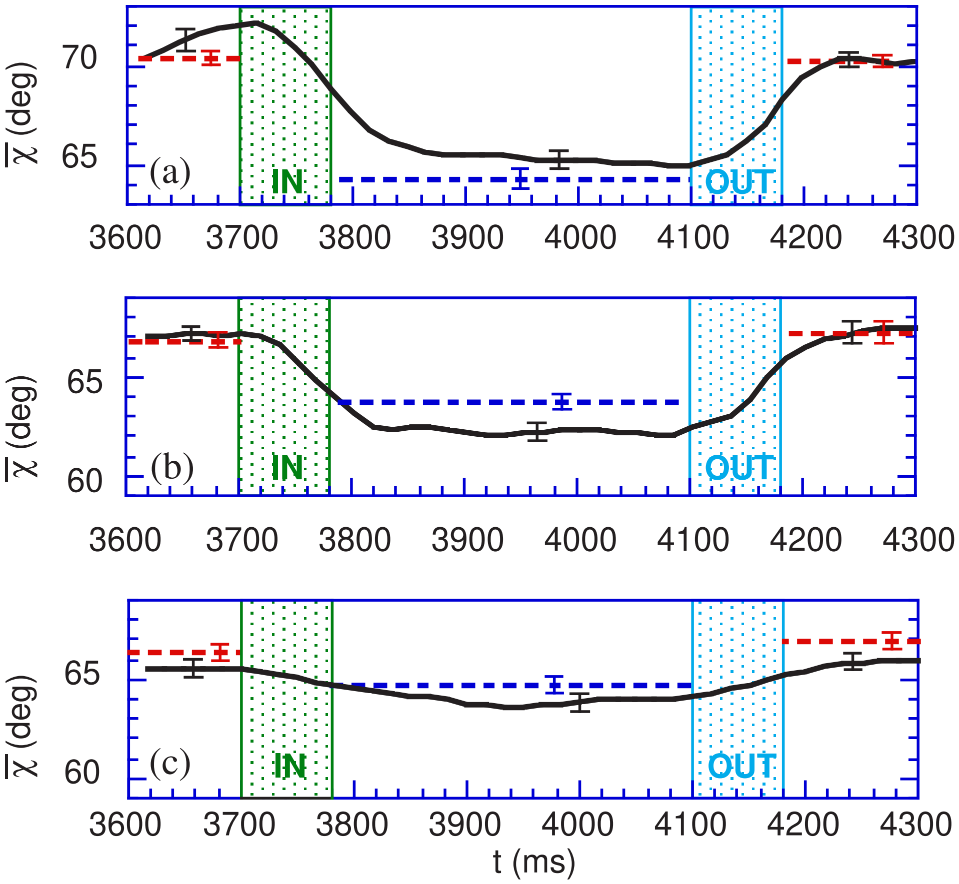

Figure 5.6: *Mean of the pitch angle distribution as a function of time for the 90° lost alpha detector signals shown in Fig. 5.4. Error bars based on one standard deviation in data scatter.*

with the exception, of the time interval between the IN and OUT shift in the 1.4 MA discharge shown in Fig. 5.6(b). Again, this correlates to the anomalous signal seen in Fig. 5.4(b).

Fig. 5.7 shows the actual pitch angle distribution for the 1.4 MA shifted discharge and its baseline comparison shot, integrated over the time of the anomalous loss between the shifts (3.9 to 4.1 s). The dashed curve labeled (a) is the baseline distribution renormalized to the peak of the shifted distribution to show that the shifted distribution is significantly narrower than that of the baseline distribution and is concentrated near the passing/trapped boundary at 59° (labeled P/T). The dashed curve labeled (b) is the sum of the baseline distribution and a modeled loss at the passing/trapped

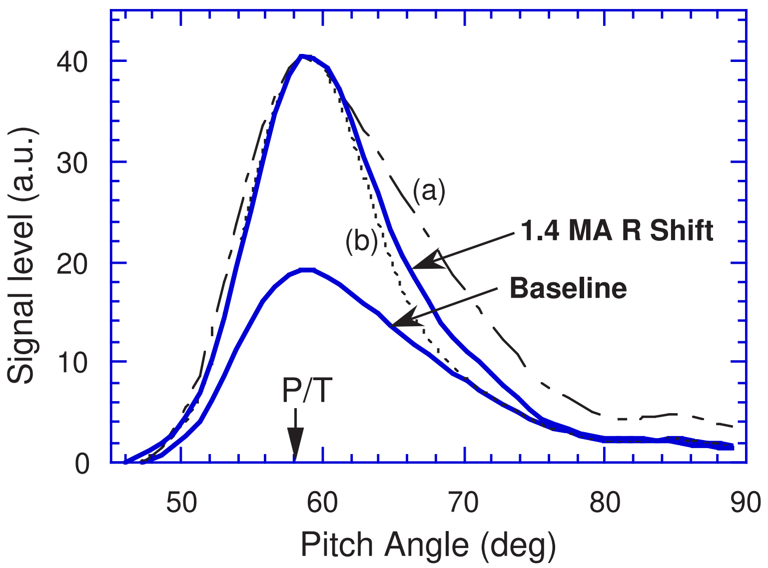

Figure 5.7: *Pitch angle distribution for period of time during anomalous loss (3.8–4.1 s). Solid lines correspond to baseline and shifted discharges. Distribution (a) is the baseline distribution renormalized to the shifted distribution for shape comparison. Distribution (b) is the sum of the baseline distribution and a distribution of α–particles lost at the passing/trapped boundary (labeled P/T) corrected for detector response.*

boundary, which takes into account the geometrical and optical resolutions of the detector. The close agreement between curve (b) and the shifted distribution is a good indication that the anomalous loss is peaked at the passing/trapped boundary, possibly extending up to $\sim 5°$ above this boundary. The pitch angle distributions for the discharges at the other currents, and for the 1.4 MA discharge before and after the shifts, display reasonably good agreement with their baseline shots, consistent with pure first orbit loss. This is true with the possible exception of the 1.8 MA discharge, which appears to exhibit behavior similar to the 1.4 MA discharge during the period between the shifts, but in a much less pronounced fashion.

5.3 Discussion

From Figs. 5.4–5.6 it is inferred that there are no additional alpha losses, besides the first orbit loss, occurring during the times of the IN and OUT shifts at the three values of plasma current. There does, however, appear to be an anomalous loss of partially thermalized α–particles at the passing/trapped boundary occurring between the time of the IN and OUT shifts at 1.4 MA.

Section 5.3.1 will offer an explanation for the absence of the expected effect of the shifts on alpha loss. Then some possible explanations for the 1.4 MA anomalous loss feature will be considered in Section 5.3.2.

5.3.1 Shift Induced Loss

Induced Toroidal Electric Field

Ref. [56] considers the effect that adiabatic compression has on α–particle orbits. The shift of the poloidal flux to smaller major radius induces a toroidal electric field which reverses direction from the high field to the low field side of the plasma. This toroidal electric field is given by:

$$E_\phi = (\partial\Psi/\partial t)_a / 2\pi Rc \tag{5.1}$$

where Ψ is the poloidal flux and the partial derivative $(\partial\Psi/\partial t)_a$ is taken in a reference frame at rest with respect to the vessel. This toroidal electric field produces an $\mathbf{E}\times\mathbf{B}$ drift that pulls the α–particles inward in major radius along with the plasma while accelerating them to higher energy. It can be shown that all α–particles gain energy regardless of their orbit classification [56]. This results from the fact that the drift surface of a co-going orbit is shifted outward in major radius (Fig. 2.1), causing the particle to spend more time being accelerated by the induced toroidal electric field on the outboard side of the plasma than being decelerated by the reversed electric field direction on the inboard side. Conversely, the drift surface of a counter-going orbit is shifted inward, causing the particle to spend more time being accelerated on the inboard side than being decelerated on the outboard side. A trapped particle orbit achieves net energy gain because the acceleration during the co-going leg is sufficient to overcome any deceleration that might be experienced due to an incomplete transit on the inboard side of the plasma during the counter-going leg. In general, $\langle E_\phi v_{\|} \rangle > 0$ (where $\langle ... \rangle$ denotes average along a particle trajectory in time) and passing particles gain more energy than trapped particles because they travel farther along the accelerating field.

Energy Gain and Shift Induced Loss

We begin with a heuristic argument to explain the lack of induced alpha loss during the IN shift. The velocity gained by marginally passing α–particles can be estimated from an approximate description of compression discussed in Ref. [56] where:

$$\frac{dv}{dt} \simeq \frac{v}{R_{ma}} \left| \frac{dR_{ma}}{dt} \right| \left[\frac{1}{2} + \frac{v_{\|}^2}{2v^2} \right] \tag{5.2}$$

where R_{ma} is the major radius of the magnetic axis. Solving for the fractional change in α–particle energy we find:

$$\frac{\Delta E}{E} = \frac{2\Delta v}{v} \simeq -\frac{\Delta R_{ma}}{R_{ma}} \left[1 + \frac{\langle E_{\|} \rangle}{E} \right] \tag{5.3}$$

where $\langle E_{\|} \rangle$ is an α–particle's parallel energy along the magnetic field averaged over the particle's orbit. For a marginally passing α–particle, which spends a large majority of its orbit bounce time near the inner midplane where its parallel velocity tends to zero, the $\langle E_{\|} \rangle$ term in Eq. 5.3 is negligible. Thus the fractional energy gain of a marginally passing α–particle is approximated by the fractional decrease in the major radius.

The change in the maximum toroidal magnetic field that an α–particle orbit reaches is related to the change in its minimum major radius by:

$$\frac{\Delta B_{max}}{B_{max}} = -\frac{\Delta R_{min}}{R_{min}} \tag{5.4}$$

Thus, assuming for the moment that an α–particle orbit shifts along with the plasma so that $\Delta R_{min}/R_{min} \simeq \Delta R_{ma}/R_{ma}$, then from Eqs. 5.3 and 5.4 we find that $E'/E \simeq B'_{max}/B_{max}$, where the prime denotes after the IN shift. Using the conservation of magnetic moment, $\mu = E_{\perp}/B = E(1-\lambda^2)/B$, where the pitch variable $\lambda \equiv v_{\|}/v = \cos\chi$, we find that for a marginally passing particle ($\lambda_{min} \simeq 0$):

$$\frac{\mu'}{\mu} = 1 = \frac{E'(1-\lambda'^2_{min})/B'_{max}}{E(1-\lambda^2_{min})/B_{max}} \simeq \frac{(1-\lambda'^2_{min})}{(1-\lambda^2_{min})} \tag{5.5}$$

From Eq. 5.5 we find that $\lambda'_{min} \simeq \lambda_{min}$, so that a marginally passing α–particle remains marginally passing, and therefore there is no alpha loss induced by the shift. But we have not given any evidence to support the assumption that an α–particle orbit moves the same amount as the plasma during the shift. Determining the new R_{min} of an α–particle orbit as a result of the R shift would require a complex equation of motion calculation taking into account the changing magnetic equilibria throughout the shift. A simpler method that avoids the need to track the entire shift is to consider the constants of the motion before and after the shift. The (μ, P_{ϕ}) space presented in Sec. 2.2.2 will be used.

Major Radius Shift in (μ, P_{ϕ}) Space

The boundaries designating orbit classifications in (μ, P_{ϕ}) space, shown in Fig. 2.2(b), shift in response to changes in plasma conditions, such as major radius and α–particle energy. However, in the absence of collisions, μ and P_{ϕ} of an individual α–particle remain fixed. Thus, by calculating the population of α–particles swept out by the shifting boundaries, the expected effect on the lost alpha signal can be estimated.

First, we consider the case of zero energy gain by an α–particle. Fig. 5.8(a) zooms in on a region of the (μ, P_{ϕ}) space for 3.5 MeV α–particles in the 1.4 MA discharge. The fixed (R,Z) parabola corresponding to the location of the 90° detector is also included. The boundaries after the IN shift are shown in lighter shading. The shifts of the boundaries, assuming no α–particle energy gain, are clearly evident. The portion of the 90° detector curve from the passing/trapped boundary to the LCFS $v_{\|} = 0$ line corresponds to first orbit loss of trapped α–particles (represented by the curve

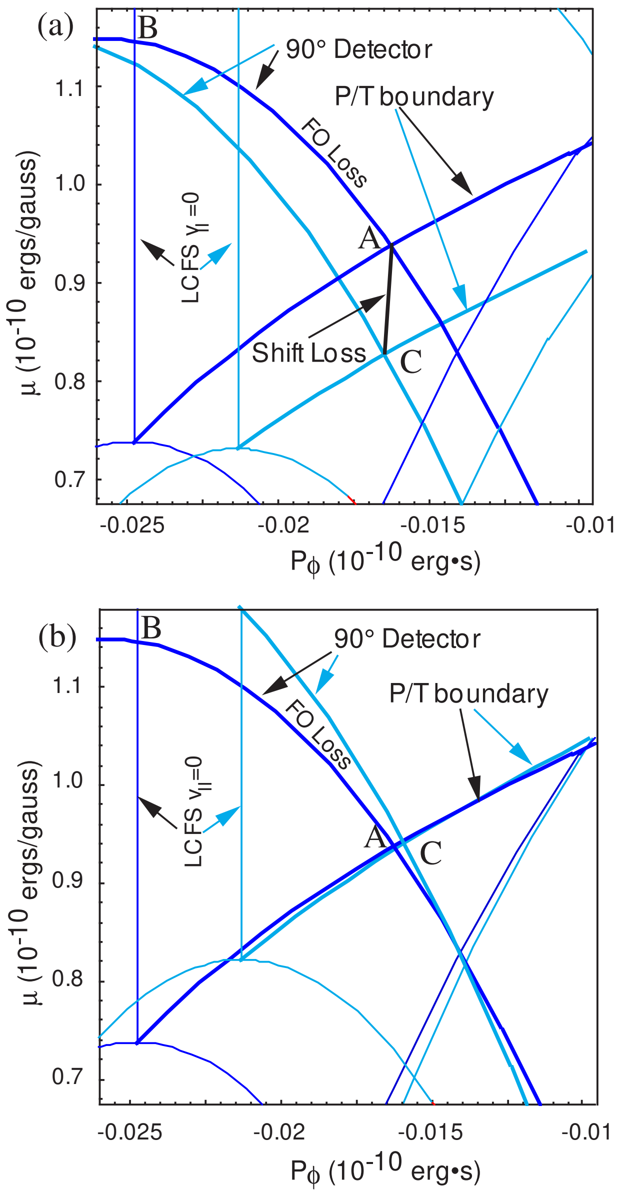

Figure 5.8: *Region of* (μ, P_ϕ) *space showing boundaries before (3.6 s) and after (3.9 s) the IN shift for the 1.4 MA discharge (after IN shift designated by light shading), assuming (a) zero energy gain and (b) 12% energy gain by* α*–particles. First orbit loss is characterized by the portion of the 90° detector parabola between the passing/trapped boundary and the* $v_{\|} = 0$ *along the LCFS (i.e. trace AB). Shift induced loss is characterized by the line connecting the intersections of the 90° detector parabola and the passing/trapped boundary before and after the IN shift (i.e. line AC). The energy gain of 12% shown in (b) is the gain needed to eliminate shift induced loss.*

AB before the shift). The intersection of the P/T boundary and the 90° detector curve represents where previously confined counter-going α–particles transition to trapped α–particles lost to 90° detector as the P/T boundary sweeps across their (μ, P_ϕ). The line AC then represents the α–particles near 3.5 MeV that contribute to any 90° detector signal increase induced by the IN shift. Alphas below the 3.5 MeV birth energy can also be lost by this mechanism. Thus, the population of α–particles that will be lost due to the shift builds up prior to the shift. The build up period is determined by the time it takes to slow down to a critical energy, below which the α–particles' banana width is too narrow to reach the 90° detector. For the 1.4 MA case in Fig. 5.8(a), the critical energy at $(r/a) = 0.3$ (within which radius over 50% of the α–particles are born) is $\approx 0.8E_0$. With an energy e-folding time of ~225 ms, it only takes ~50 ms to slow down to this energy. Thus, the α–particles lost by the shift accumulate on roughly the same time scale as they are released by the 80 ms shift.

As a rough estimate of the expected 90° detector signal fractional increase, we find:

$$\frac{\Delta Sig_{90^\circ}}{Sig_{90^\circ}} \approx \frac{W_{shift}}{W_{fo}} \frac{t_{crit}}{t_{shift}} \tag{5.6}$$

where ΔSig_{90° is the expected 90° detector signal increase, W_{shift} and W_{fo} are the source weighted loss rates induced by the shift (integrated over AC in Fig. 5.8) and from first orbit loss (integrated over AB in Fig. 5.8), respectively, and t_{crit} and t_{shift} are the time to slow down to the critical energy and shift time, respectively. For the 1.4 MA case depicted in Fig. 5.8(a), in which it is assumed that the α–particles gain no energy during the shift, an estimated 50% increase is predicted. This result was used for the expected lost alpha signal increase of Fig. 5.3(c) during the IN shift.

The predicted 90° detector signal increase is reduced if the α–particles are allowed to gain energy during the IN shift, as discussed in the previous section. The energy gain required to totally eliminate the shift-induced signal increase is found by increasing the α–particle energy until there is no longer a shift of the P/T boundary. Fig. 5.8(b) shows that this case occurs for $\sim$ 12% α–particle energy gain for the 1.4 MA case. By plotting the P/T boundary for other α energies capable of reaching the 90° detector it is found that the $\sim$ 12% energy gain necessary to eliminate the signal increase is approximately independent of α–particle energy in the range 1.0–3.5 MeV.

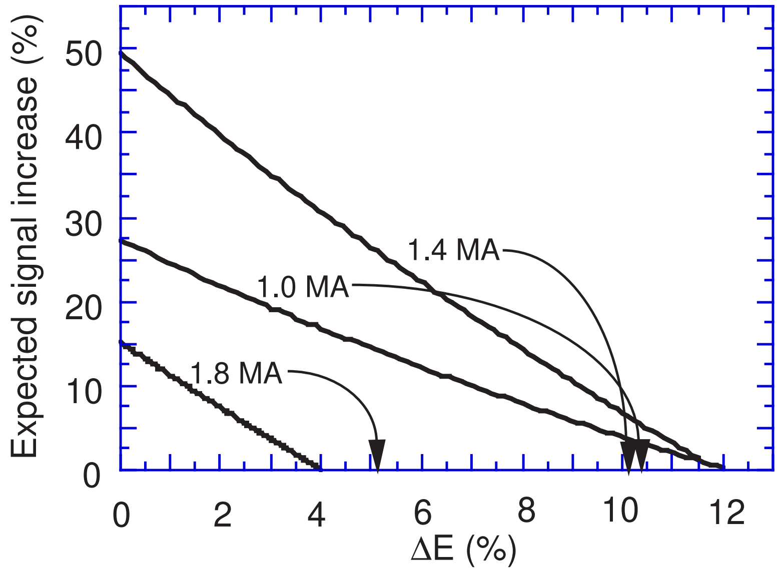

Figure 5.9: *Predicted 90° detector signal increase as a function of energy gained by α–particles for each of the three currents. The energy gain, estimated from Eq. 5.3, is shown by the arrows.*

This is also the energy gain required to keep the R_{min} point at the same r/a such that the α–particle orbit maintains its position in the plasma with respect to magnetic flux surfaces throughout the R shift. This result is consistent with the heuristic argument of the last section.

Fig. 5.9 shows the predicted 90° detector signal increase as a function of α–particle energy gain estimated using Eq. 5.6. In both the 1.0 and 1.4 MA cases, the shift-induced loss is eliminated at $\sim 12\%$ α–particle energy gain, while the 1.8 MA case cuts off at only $\sim 4\%$ due to the smaller shift range. The energy gain predicted by Eq. 5.3 is depicted by the arrows in Fig. 5.9 for each of the three values of plasma current. It is seen that the energy gained by alpha particles during the IN shift should have a significant effect on the predicted 90° detector signal increase. While the models used are only approximate, they are sufficient to show that the shift-induced alpha loss is reduced by a factor of five or more when the α–particle energy gain is taken into account. While the absolute magnitude of the calculated signal increase is probably only accurate to within a factor of 2 or 3, the important point is that the energy gained by an α–particle is near the point at which no shift-induced alpha loss is expected.

Additional effects, not taken into account in this model, would tend to further reduce the predicted shift-induced loss. For instance, collisional nonprompt loss has the effect of reducing the population of α–particles in a boundary layer region near the passing/trapped boundary because these particles can pitch angle scatter across to the trapped side of the boundary and become lost. So these particles, which would have been the first to be lost due to the shift, are no longer available to be lost during the shift. Furthermore, the α–particles that are swept out by the boundary have a non-zero average $E_{||}$ resulting in larger energy gain according to Eq. 5.3 and, as can be seen in Fig. 5.9, cause a further reduction in shift-induced loss.

The 1.0 MA case warrants further discussion. The expected signal increase for zero α–particle energy gain is smaller than in the 1.4 MA case. This is because in the 1.0 MA discharge, first orbit loss α–particles can come from the plasma core where the source profile is peaked. In the 1.4 MA case, first orbit loss α–particles can only come from as close as $r/a \approx 0.2$, while the shift-induced α–particles can come from closer in to the core. Thus the shift induces a larger effect in the 1.4 MA case. Also, the shift-induced α–particles in the 1.0 MA case are lost at lower energies since fattest banana α–particle orbits near the birth energy have banana widths that are too large, causing them to strike the vessel on the inboard side. For shift-induced lost α–particles to strike the 90° detector at 1.0 MA, their energy must be $< 0.7\ E_0$. Thus a similar size shift induced loss in the 1.0 and 1.4 MA discharges would lead to a lower mean gyroradius in the 1.0 MA case, making it easier to diagnose.

Uncertainties

Several simplifying assumptions were made in calculating the shift-induced loss levels in Fig. 5.9. For instance, it was assumed that the weighting factors of Eq. 5.6 could be represented by the source strength at the orbits' outer midplane crossing point (i.e. the point of closest approach to the magnetic axis where the source is peaked), rather than integrating the source term along entire orbits. Although a counter-going marginally passing orbit is different from a trapped orbit, the steep peakedness of the source profile combined with the shift of alpha drift surfaces away from flux surfaces (Fig. 2.1), ensures that the alpha distribution of either orbit type is dominated by the contribution from near this OMP crossing point. Furthermore, since the time to slow down to the critical energy, t_{crit}, is short compared to the slowing down time, (τ_{SD}), it was assumed that it would be sufficient to do the calculation at one energy (i.e. the birth energy, or, in 1.0 MA case, the maximum energy at which alphas can reach the 90° detector). These factors combine to make the calculated signal increase accurate to within a factor of 2 or 3. The energy gain at which the shift induced loss is eliminated, however, should be accurate to within a few percent as determined by uncertainty in the magnetic equilibria.

5.3.2 Anomalous Loss Between the Shifts

Another result of this experiment is the unexpected loss of partially thermalized α–particles ($E \approx 0.8E_0$) at the passing/trapped boundary in between the time of the IN and OUT shifts at 1.4 MA. This loss is similar to the loss feature know as 'delayed' loss (Sec. 4.4.2) [40] observed in small major radius ($R_0 = 2.45m$) deuterium plasmas at high plasma current ($I_p \geq 1.8$ MA) with the 90° lost alpha scintillator detector. An anomalous loss consistent with 'delayed' loss was also observed in deuterium-tritium plasmas using the Alpha Collector probe (Chapter 4). The mechanism causing this loss is not yet understood. However, 'delayed' loss is observed to occur at a pitch angle $\sim 10°$ above the passing/trapped boundary in deuterium, and has not been observed in DT plasmas with the 90° lost alpha scintillator detector used in this experiment. The large pitch angle of 'delayed' loss requires a large radial step diffusive process to allow α–particles to reach the 90° location without having been previously scraped off at the outer midplane.

A loss at the passing/trapped boundary, such as the anomalous loss at 1.4 MA, does not necessarily require an explanation based on large radial diffusion, since any mechanism that can cause marginally passing α–particles to cross over the boundary is sufficient. Such mechanisms that have been explored in detail are ICRH induced loss [20], collisional nonprompt loss [15], and MHD induced loss [40]. Since there was no RF in these discharges, ICRH can be ruled out. And although the collisionality of these plasmas went up after the IN shift, it will be shown that collisional loss is such a small contributor to total alpha loss that it isn't expected to be significant during these 'steady state' conditions. These discharges were designed to avoid MHD activity, and it will be shown that there is no correlation between the anomalous loss and what little MHD there is in these discharges. But first, the possibility that the anomalous loss signal is a result of differences in the source and q profiles between the shifted and baseline discharges is examined.

Source and q Profiles

The following arguments regarding the effect of source and q profiles on the mean gyroradius, neutron normalized alpha flux, and pitch angle distribution, support the supposition that the additional alpha loss seen in the 1.4 MA R shifted discharge between the time of the IN and OUT shift is an actual anomalous loss of partially thermalized alphas, and not pure first orbit loss mistaken as such due to instrumental error.

The pitch angle distribution and flux of first orbit alpha loss is dependent on the alpha source and plasma current (or equivalently, q) radial profiles. However, these profiles should not have an effect on the gyroradius distribution of first orbit loss since this loss occurs at a fixed energy of 3.5 MeV ($\pm \sim$0.5 MeV spread for Doppler shift). Thus, it is not expected that differences in these profiles could account for the $\sim$ 0.2 cm decrease in mean gyroradius seen for the shifted discharge in Fig. 5.5(b) if this observation is to be consistent with first orbit loss. But there could be instrumental errors not taken into account in the error bars in this figure. In particular, it is possible that the model used to map a (ρ, χ) grid onto the scintillator image, which is used to transform alpha impact position on the scintillator to gyroradius and pitch angle (Sec. 2.5.1), is slightly misaligned. This could cause differing pitch angle distributions with the same alpha loss energy to result in slightly differing apparent gyroradius distributions once the transformation is applied.

Fig. 5.10 shows the original 1.4 MA pitch angle distributions of Fig. 5.7 (averaged

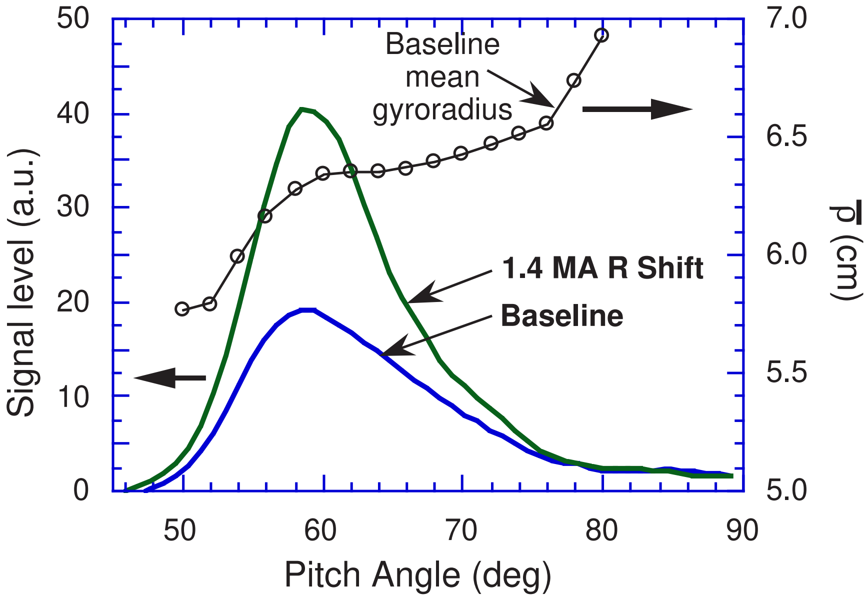

Figure 5.10: *Baseline and shifted pitch angle distributions averaged over 3.9–4.1 s (left scale) and mean gyroradius of the baseline discharge as a function of pitch angle averaged over 2° bins (right scale).*

over the time period of the anomalous loss, 3.9–4.1 s), along with the mean gyroradius of the baseline distribution as a function of pitch angle. The mean gyroradius was calculated for 2° wide bins in pitch angle. Assuming that the energy distribution of the loss is independent of pitch angle (e.g. first orbit loss), one would also expect that the mean gyroradius would be independent of pitch angle. The misalignment of the mapping model must then be responsible for the pitch angle dependence of the mean gyroradius seen in Fig. 5.10. Since the shifted pitch angle distribution is more concentrated at lower pitch angle (where the apparent mean gyroradius is also lower) than the baseline is, the misalignment of the mapping model may cause it to have a lower apparent mean gyroradius. Using the mean gyroradius curve of Fig. 5.10 to calculate the mean gyroradius of the baseline pitch angle distribution, averaged over 50–80° in pitch angle, results in a mean gyroradius value of 6.30 cm, in agreement with the baseline mean gyroradius in Fig. 5.5(b) between the IN and OUT shift. To determine if the pitch angle distribution of the 1.4 MA shifted discharge could cause first orbit loss at 3.5 MeV to appear to have a lower mean gyroradius, the same binned mean gyroradius distribution (i.e. corresponding to first orbit loss) was applied to this

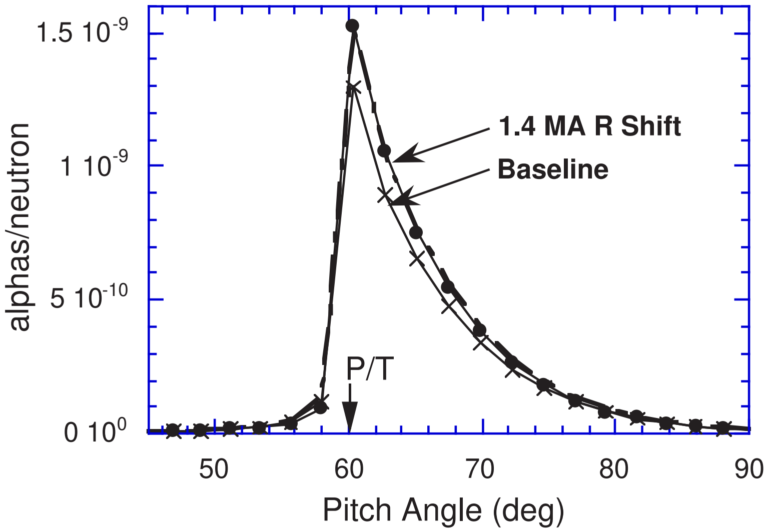

Figure 5.11: *Pitch angle distributions for the baseline (x's) and shifted (circles) discharges calculated using the Lorentz ORBIT code. The baseline distribution renormalized to the peak of the shifted distribution is shown by the dashed line.*

discharge in the same manner, resulting in a mean gyroradius value of 6.29 cm, only 0.01 cm less than the baseline value. Therefore, the differing pitch angle distributions, combined with a misaligned mapping model, do not account for the ~ 0.2 cm lower mean gyroradius observed for the shifted discharge seen in Fig. 5.5(b).

To further counter the argument that differing source and q profiles are responsible for the anomalous loss features, the TRANSP [16] calculated q profile and the Abel inverted source profile generated from measurements made with the neutron collimator [59] were used to calculate the alpha loss to the 90° detector for the 1.4 MA baseline and shifted discharges at 3.95 s (i.e. during the time of the anomalous loss) using the Lorentz ORBIT code (Sec. 4.2). Fig. 5.11 shows the calculated pitch angle distributions. These distributions are narrower and more sharply peaked at the passing/trapped boundary than those of Fig. 5.7 because they are not 'smeared' out by the detector response, which can be modeled by a convolution of these calculated distributions with a Gaussian response function. The slightly differing source and q profiles result in an $\sim 18\%$ larger alpha loss for the shifted discharge as compared to the baseline discharge. This is in consistent with the $\sim 13\%$ spread between the shifted and baseline first orbit calculations at 3.95 s shown in Fig. 5.4(b), which were done using the TRANSP calculated source profile as input rather than the neutron collimator generated source profile. So the calculated increase in the first orbit loss of $< 20\%$ is significantly less than the observed 70% increase. To compare the shapes of the distributions, the baseline distribution is renormalized to the peak of the shifted distribution (shown by the dashed line), similar to what was done in Fig. 5.7. The shapes of the baseline and shifted distributions are clearly in agreement. There is no peaking of the shifted distribution at the passing/trapped boundary with respect to the baseline distribution as was seen in the observed distributions of Fig. 5.7(b). Therefore, the observed 1.4 MA loss is not consistent with the predicted first orbit loss.

Collisional Loss

To investigate the effect of collisionality, the Hamiltonian guiding center drift orbit Monte Carlo code, ORBIT [43], was used to simulate the slowing down process of α–particles under the conditions of the 1.4 MA R shifted discharge. One thousand particles were allowed to slow down from 3.5 to below 2.5 MeV (0.7 E_0) while being acted upon by collisions (Sec. 2.4.1) and stochastic TF ripple diffusion (Sec. 2.3.2). Stochastic ripple diffusion (SRD) is a collisionless process which produces a radial step near the banana tip of those trapped particles that meet a particular threshold criteria [12]. Collisions can act to enhance this loss mechanism by allowing α–particles on previously non-stochastic orbits to exceed this threshold, leading to a synergistic effect [13].

The results from the ORBIT code are presented in Fig. 5.12. For the conditions before the shift, when R=2.6 m, a global alpha loss of $\sim 21\%$ is found, as shown by the first bar of Fig. 5.12(a) where a total of 213 of the original 1000 particles are lost. Of this loss, $\sim 26\%$ is nonprompt (i.e. not first orbit loss). However, most of this nonprompt loss occurs near the outer midplane, as is typical for SRD since it is a small step-size radial diffusive process and must first scrape off at the outer midplane where outwardly diffusing orbits first hit the wall. Only about 7% of the alpha loss to a region 10° either side of the 90° wall location (corresponding to only 2 of the

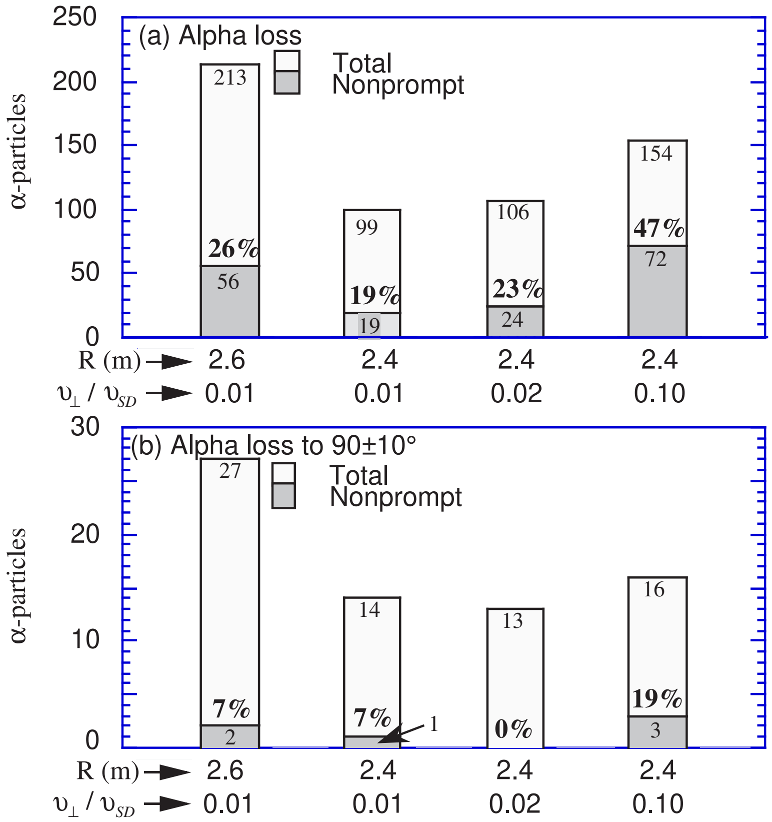

Figure 5.12: *Alpha loss calculated using the guiding center ORBIT code for the 1.4 MA discharge before (R=2.6 m) and after (R=2.4 m) the IN shift. After the IN shift was run for three values of collisionality. Bars represent (a) total loss to the wall and (b) loss to the bottom of the vessel at 90 ± 10°. Total (prompt plus nonprompt) and nonprompt amounts are labeled (out of original 1000 alphas tracked), along with the percentages that make up nonprompt loss.*

original 1000 particles) is nonprompt as seen in the first bar of Fig. 5.12(b). For the conditions after the IN shift, when R=2.4 m (i.e. during the anomalous loss), and assuming the same collisionality as the previous case, a global alpha loss of $\sim$ 10% is found, of which $\sim$ 19% is nonprompt (second bar of Fig. 5.12(a)). The lower total loss is due to the fact that the magnetic flux surfaces, and hence the alpha orbits, are farther from the walls in a smaller major radius plasma. But still, only about 7% of the alpha loss to a region 10° either side of the 90° wall location (only 1 of original 1000) is nonprompt (second bar of Fig. 5.12(b)).

Of course the effect of compression on the collisionality must be considered. The relevant quantity is the collisionality ratio of the 90° scattering rate to the slowing down rate, $\nu_\perp/\nu_{SD}$, since this determines the degree of pitch angle scattering in a slowing down time. This quantity is found to increase on the order of 30% due to the compression. To be conservative, ORBIT was run for the conditions during the anomalous loss with the 90° scattering time halved, so that the collisionality ratio was doubled. The global alpha loss increased slightly to $\sim$ 11% (third bar of Fig. 5.12(a)), the increase being due to the increase in nonprompt loss (collisional and SRD) which made up $\sim$ 23% of the loss. However, none of the nonprompt loss hit the wall 10° either side of the 90° location (third bar of Fig. 5.12(b)). Due to the small statistical sample this is not significantly different then the previous two results where there were 2 and then only 1 nonprompt alphas striking this region. What is significant is that this result did not increase to $\sim$ 70% of first orbit loss in this region (i.e. $\sim$ 9 of original 1000 particles) as is the case for the observed anomalous loss. Even increasing the collisionality ratio by a factor of 10 resulted in only $\sim$ 19% of the alpha loss to a region 10° either side of the 90° wall location (3 of original 1000) being nonprompt (fourth bar of Fig. 5.12(b)). Thus nonprompt collisional loss does not appear to be a viable explanation for anomalous loss occurring in between the shifts at 1.4 MA.

MHD

The discharges of this experiment were done at relatively low NBI power (i.e. 10 MW) to avoid MHD activity. However, an inspection of measurements made with the Mirnov magnetic probes [60] and the multichannel electron cyclotron emission (ECE) polychromator arrays [61] reveal a low level of MHD in several of the discharges. For instance, the Mirnov signals indicate the presence of a $\sim$ 60 kHz mode near the radius of maximum pressure gradient, features characteristic of the kinetic ballooning mode (KBM) [62], in the 1.0 MA shifted discharge beginning at the end of the IN shift at 3.77 s, and persisting past the end of the OUT shift. KBMs have been observed to cause alpha particle loss at the passing/trapped boundary resulting in an increased loss of up to three times first orbit loss to the 90° detector in high β (plasma pressure/magnetic pressure), high power (P_B = 21 MW, P_{fusion} = 5.5 MW)

DT plasmas [17]. However, the alpha loss of this 1.0 MA discharge is in agreement with its baseline comparison discharge which did not exhibit MHD activity, indicating that the KBMs of this lower power ($P_B = 10$ MW, $P_{fusion} = 1.1$ MW) discharge were probably too small to cause significant alpha loss.

The 1.4 MA shifted discharge, which produced the anomalous alpha loss results, was done twice to ensure reproducibility. Nearly identical alpha loss results were obtained in both shots. However, one of these discharges exhibits a ~ 50 kHz mode, also consistent with the KBM, whereas the other discharge exhibits a weak 3/2 mode at ~ 10 kHz. Thus, there does not appear to be a correlation of the anomalous loss with MHD activity.

5.4 Summary, Conclusions, and Suggestions for Future Work

See Sec. 6.3.

Chapter 6

Conclusion

6.1 Introduction

The development of DT fusion tokamak reactors as a long term energy option will require an understanding of the behavior of alpha particles in thermonuclear plasmas. While the confinement of alpha particles is necessary to achieve ignition, a more critical concern is that the loss of these energetic particles could cause damage to the first wall of a reactor.

This thesis covered two experiments investigating separate aspects of escaping alphas in TFTR. Chapters 3 and 4 described the development and results of the alpha collector probe. Chapter 5 described the major radius shift experiment done to investigate the effect on alpha loss. This chapter summarizes these two experiments and draws some conclusions. Suggestions for future experimental work are given here in the event that the TFTR experimental campaign is restarted or that similar results are observed on other machines. However, the suggestions for further modeling do not require an operational tokamak.

6.2 Alpha Collector

6.2.1 Summary

Escaping α–particles have been collected from four DT shots in stacks of thin nickel foils located within the alpha collector probe on TFTR. The subsequent melting of the foils in a closed volume and measurement of the released He as a function of layer depth yields a lost alpha energy distribution, with better than 20% energy resolution. Two rows of eight collimating ports each provide full 180° pitch angle coverage (with the exception of self-shadowing of very deeply trapped particles by the probe head), but with limited pitch angle resolution. The foil deposition technique employed by the alpha collector is accurate to within ±10% at fluences above $\sim 10^9$ alphas, providing an absolutely calibrated measurement to check alpha loss models and to cross calibrate other detection methods. The lack of electronics and optics gives it good immunity to high neutron fluxes, and the use of a mass spectrometer in the analysis allows for positive ion identification. Although these features make the alpha collector an attractive diagnostic for future fusion reactors, several disadvantages may make other methods preferable. For instance, the alpha collector has no intrinsic time resolution, requires accessibility to retrieve the exposed foils, and requires a long turn around time between exposure and analysis.

The alpha collector has been used to measure escaping alphas in 2.45 m plasmas for two discharges at a plasma current of 1.0 MA, and two discharges at 1.8 MA. For the 1.0 MA discharges, the total alpha fluence, energy distribution, pitch angle distribution, and radial distribution are all in good agreement with the first orbit loss model, and with the signals from the nearby 90° lost alpha scintillator detector, with the exception of a small anomalous loss feature at an energy below $\sim$2 MeV. The results of the 1.8 MA discharges, however, display a large anomalous loss feature, in addition to first orbit loss, with an alpha fluence a factor of $\sim$6 larger than the predicted first orbit loss. This anomalous loss is broadly peaked at an energy of $\sim$2.5 MeV. From this partial thermalization it can be inferred that this loss is 'delayed' with respect to alpha production by about one third of the energy e-folding time. The anomalous loss occurs for particles that are co-going at the detector which are more trapped than the fattest banana orbit, and it exhibits a strong radial dependence which may be due to RF limiter shadowing, or an indication of a diffusive loss mechanism. The signals of the 90° scintillator detector during these discharges, however, are in agreement with the first orbit loss model and do not display any sign of this anomalous loss.

6.2.2 Conclusions

The qualitative characteristics of the anomalous loss detected at 1.8 MA with the alpha collector probe are similar to those of the 'delayed' loss feature identified in DD plasmas with the 90° scintillator detector [40]. This implies that they may be due to the same loss mechanism, although, it is not understood why the anomalous loss does not appear on the scintillator detectors in DT.

The strong radial dependence of the anomalous loss, a factor of three decrease in measured fluence from the upper to the lower row of collimating ports, suggests a radial diffusive process, which should cause a reduction in alpha flux due to scrape-off outside the radius of an obstacle such as the RF limiters. However, to go from a marginally confined orbit, which just misses the outer midplane, to the anomalous loss orbit which intercepts the detector, the alpha banana tip would have to jump at least 15 cm. Such a large step-size results in very little radial variation over the 1.1 cm separation between the upper and lower rows of collimating ports. If it is assumed that orbits exist that intercept the RF limiters at the bottom of the vessel first, rather than at the midplane, then a small step-size of $\sim$0.2 cm can account for the factor of three drop. However such orbits require that the alpha energy be below the minimum detectable energy of $\sim$0.5 MeV. Thus there appears to be an inconsistency between the radial dependence and the diffusive step-size required to bring an α–particle to the detector, making it difficult to develop a model which accounts for the characteristics of the anomalous loss. This inconsistency has led us to question our basic understanding of α–particle orbits in TFTR. In particular, improved modeling of the magnetic fields in the vacuum gap region between the last closed flux surface and the wall may reveal that outwardly diffusing alphas can scrape off at the bottom of the vessel, as well as at the outer midplane. This might provide a mechanism for alphas to reach the alpha collector through the relatively small step-size diffusive process of stochastic ripple diffusion. Such a small step-size diffusive process would be consistent with the absence of the anomalous loss to the 90° scintillator detector, since it is located nearly a cm farther outside the RF limiter radius than the lower row of ports on the alpha collector.

Several possible mechanisms have been considered in an attempt to explain the anomalous loss. The explanation that is most consistent with the observations is charge exchange loss, in which previously confined α–particle orbits transition to prompt loss orbits as a result of electron capture from hydrogen-like carbon impurities. Further work is needed to quantify this loss mechanism and to determine if its effects should be evident to other escaping and confined alpha diagnostics. The most straight forward approach is to develop a guiding center Monte Carlo code to take into account the probabilities for charge exchange and reionization as a function of alpha energy and minor radius (since plasma and impurity density depend on minor radius). However, the absence of the anomalous loss on the scintillator detectors and its radial dependence do not appear to be consistent with the large step-size diffusion that would be associated with this loss process.

In the design of a fusion reactor it is necessary to be able to predict the alpha wall loading in order to prevent hot spots. Thus, the global alpha loss and its distribution to the first wall is more important than the loss to a localized detector. Unfortunately, it is difficult to make wall loading predictions based on the loss to a single detector. This is because the effective wall area of a given detector (i.e. the area generated by projecting the trajectories of the detected particles onto the first wall as if they had not been stopped by the detector) may vary widely between different types of alpha loss. Although the detected anomalous loss is significantly larger than the predicted first orbit loss, this loss may be preferentially concentrated in the detector (due to a large effective wall area), resulting in a lower actual wall loading than might be expected. For instance, for a small-step diffusive loss mechanism, the effective wall area generated by a detector positioned inside the RF limiter radius can be relatively large since the detector can scrape-off particles that would otherwise have spread over a large area owing to the randomization of the diffusion process.

Similarly, without knowing the loss mechanism, it is difficult to estimate the global alpha loss based on a localized detector since this measurement provides no information regarding poloidal distribution. Assuming that the mechanism responsible for the anomalous loss is impurity charge exchange, then the gc-ORBIT code estimate of $\sim 20\%$ global loss, which is $\sim$8 times the first orbit loss prediction (Sec. 4.5.4), can be taken as a 'best guess' of the upper limit of the global anomalous alpha loss. However, this may be a gross over-estimate due to the potentially large uncertainties in the charge exchange cross section and the method used to quantify this loss mechanism. As of yet, no other diagnostic results have suggested the existence of such a loss. As for a lower limit of the global anomalous alpha loss, it is conceivable that this loss is very poloidally localized to the bottom of the vessel or that it is concentrated in the detector (due to a large effective wall area), resulting in an insignificant global loss in comparison to first orbit loss.

6.2.3 Suggestions for Future Work

Further work is needed to characterize the anomalous alpha loss seen in this experiment. Scans in plasma current, major radius, beam power, and radial position could shed more light on the anomalous loss. For instance, it should be possible to determine if the small low energy loss feature at 1.0 MA is related to the anomalous loss at 1.8 MA through a plasma current scan. And probe head design changes could improve the quality of the measurement. Such changes could include narrower collimating ports to improve pitch angle resolution, thinner nickel foils to improve energy resolution, and programmable shutters over the foils to improve time resolution.

Further modeling, particularly of the charge exchange loss mechanism, might provide an explanation for the anomalous loss. Efforts to correctly model the magnetic field in the vacuum gap region between the last closed flux surface and the wall [44] might produce orbits that scrape off at the bottom of the vessel rather than at the outer midplane. This could provide a mechanism for alphas lost through stochastic ripple diffusion to reach the alpha collector at the bottom of the vessel.

6.3 Major Radius Shift Experiment

6.3.1 Summary and Conclusions

It has been observed that major radius shifts do not induce additional alpha loss in TFTR, as had been expected. Subsequent modeling of the alpha particle dynamics revealed that the energy gained by marginally passing α–particles during a compression is probably sufficient to avoid mirroring as they move to higher magnetic field, such that they remain passing and confined. However, the major radius shift experiment uncovered a new unexpected loss of partially thermalized ($E \approx 0.8E_0$) α–particles being lost at the passing/trapped boundary. Increased pitch angle scattering of α–particles across the passing trapped boundary in the post-compression, hotter, denser plasma does not appear to be sufficient to explain this anomalous loss. Observed MHD activity also does not appear to be correlated with this anomalous loss.

6.3.2 Suggestions for Future Work

Future experimental efforts should attempt to further characterize the anomalous loss. This can be accomplished by varying the shift range and rate and by conducting a finer plasma current scan. The delay time after the IN shift could be extended to see if the anomalous loss subsides as the plasma approaches steady state. Further theoretical modeling could improve the alpha loss predictions during the shifts. Modification of a guiding center code such as ORBIT to track the orbits of α–particles throughout the shifts could provide a direct numerical calculation. But priority should be placed on understanding the anomalous loss at 1.4 MA.

Bibliography

[1] A. Einstein, H. A. Lorentz, H. Minkowski, and H. Weyl, *The Principle of Relativity.* Dover, 1952.

[2] K. M. McGuire *et al. Phys. Plasmas*, vol. 2, p. 2176, 1995.

[3] L. A. Artsimovich *Nucl. Fusion*, vol. 12, p. 215, 1972.

[4] N. J. Fisch *Phys. Plasmas*, vol. 2, p. 2375, 1995.

[5] W. W. Heidbrink *et al. Nucl. Fusion*, vol. 34, p. 535, 1994.

[6] J. A. Rome and Y.-K. M. Peng *Nucl. Fusion*, vol. 19, p. 1193, 1979.

[7] C. T. Hsu and D. J. Sigmar *Phys. Fluids B*, vol. 4, p. 1492, 1992.

[8] S. J. Zweben *et al. Nucl. Fusion*, vol. 30, p. 1551, 1990.

[9] S. J. Zweben *et al. Nucl. Fusion*, vol. 35, p. 893, 1995.

[10] R. L. Boivin *et al. Nucl. Fusion*, vol. 33, p. 449, 1993.

[11] O. A. Anderson and H. P. Furth *Nucl. Fusion*, vol. 12, p. 207, 1972.

[12] R. J. Goldston *et al. Phys. Rev. Lett.*, vol. 47, p. 647, 1983.

[13] M. Redi *et al. Nucl. Fusion*, vol. 35, p. 1191, 1995.

[14] S. J. Zweben *et al. Nucl. Fusion*, vol. 35, p. 1445, 1995.

[15] C. S. Chang *et al. Phys. Plasmas*, vol. 1, p. 3857, 1994.

[16] R. Hawryluk *et al.* in *Proc. Course Varenna, 1979, CEC, Brussels*, vol. 1 of *Physics of Plasmas Close to Thermonuclear Conditions*, p. 19, 1980.

[17] D. S. Darrow *et al. Phys. Plasmas*, vol. 3, p. 1875, 1996.

[18] R. Nazikian *et al. Phys. Rev. Lett.*, vol. 78, p. 2976, 1997.

[19] R. B. White *et al. Phys. Plasmas*, vol. 2, p. 2871, 1995.

[20] D. S. Darrow *et al. Nucl. Fusion*, vol. 36, p. 1, 1996.

[21] S. J. Zweben *et al. Nucl. Fusion*, vol. 29, p. 825, 1989.

[22] D. S. Darrow *et al. Rev. Sci. Instrum.*, vol. 66, p. 476, 1995.

[23] H. W. Herrmann *et al. Rev. Sci. Instrum.*, vol. 66, p. 351, 1995.

[24] H. W. Herrmann *et al. Nucl. Fusion*, p. in press, 1997.

[25] R. A. Langley *Bull. Am. Phys. Soc.*, vol. 29, p. 1309, 1984.

[26] R. Bastaz *et al. Rev. Sci. Instrum.*, vol. 61, p. 3199, 1991.

[27] E. V. Carruthers *et al. J. Nucl. Mater.*, vol. 176/177, p. 1027, 1990.

[28] J. Zhu *et al. Nucl. Instr. and Meth.*, vol. B59/60, p. 168, 1991.

[29] J. F. Ziegler, *Helium: Stopping Powers and Ranges in All Elemental Matter.* Pergamon Press, Oxford, 1977.

[30] A. E. Pontau, C. B. Layne, and W. Bauer *J. Nucl. Mat.*, vol. 103, p. 535, 1981.

[31] G. P. Chong *et al. Bull. Am. Phys. Soc.*, vol. 39, p. 1675, 1994.

[32] G. P. Chong, "Measurement of helium in nickel foils from the tftr alpha collector probe," Master's thesis, University of Toronto Institute for Aerospace Studies, 1995.

[33] K. Y. Wong *et al. Fusion Engineering and Design*, vol. 16, p. 159, 1991.

[34] S. J. Zweben *et al. Phys. Plasmas*, vol. 1, p. 1469, 1994.

[35] G. J. Sadler *et al. Nucl. Fusion*, vol. 35, p. 1609, 1995.

[36] J. Felt *et al. Rev. Sci. Instrum.*, vol. 61, p. 3262, 1990.

[37] J. F. Ziegler, J. P. Biersack, and U. Littmark, *The Stopping and Range of Ions in Solids.* Pergamon Press, Oxford, 1985.

[38] W. Choe *personal commuication*, 1996. Princeton Plasma Physics Laboratory.

[39] L. C. Johnson *et al. Rev. Sci. Instrum.*, vol. 66, p. 894, 1995.

[40] S. J. Zweben *et al. Nucl. Fusion*, vol. 33, p. 705, 1993.

[41] S. J. Zweben *et al. Rev. Sci. Instrum.*, vol. 63, p. 4565, 1992.

[42] S. T. Wang and S. J. ZWEBEN, "Model of alpha particle diffusion in the outer limiter shadow of tftr," PPPL Report 3186, Princeton Plasma Physics Laboratory, 1996. submitted to Nucl. Fusion Lett.

[43] R. B. White *Phys. Fluids B*, vol. 2, p. 845, 1990.

[44] V. Yavorski *personal commuication*, 1996. Inst. for Nuclear Research, Kiev.

[45] S. J. Zweben *et al.* in *14th Int. Conf. on Plasma Physics and Controlled Nuclear Fusion Research, Wurzburg, 1992*, vol. 1, p. 363, IAEA, Vienna, 1992.

[46] H. E. Mynick in *Theory of Fusion Plasmas*, (Proc. Joint Varenna-Lausanne Int. Workshop Chexbres, 1988), Editrice Compositori, Bologna, pp. 385–400, 1988.

[47] R. E. Olson *Phys. Lett.*, vol. 71A, p. 341, 1979.

[48] R. A. Hulse *Nucl. Technol. Fusion*, vol. 3, p. 259, 1983.

[49] R. E. Olson *Phys. Rev.*, vol. A16, p. 531, 1977.

[50] T. G. Winter *Phys. Rev*, vol. A47, p. 264, 1993.

[51] T. G. Winter *personal commuication*, 1996. Pennsylvania State University, Wilkes-Barre Campus.

[52] R. F. Heeter *Bull. Am. Phys. Soc.*, vol. 40, p. 1768, 1995.

[53] R. A. Phaneuf *et al.*, "Atomic data for fusion, vol. v," ornl-6090, Oak Ridge National Laboratory, 1987.

[54] Z. Bödy and J. Csikai, "Handbook on nuclear activation data," IAEA Tech. Report Series 273, International Atomic Energy Agency, Vienna, 1987. 261-304.

[55] H. P. Furth and S. Yoshikawa *Phys. of Fluids*, vol. 13, p. 2593, 1970.

[56] N. N. Gorelenkov *Sov. J. Plasma Phys.*, vol. 16, p. 241, 1990.

[57] H. W. Herrmann *et al. Bull. Am. Phys. Soc.*, vol. 39, p. 1675, 1994.

[58] H. W. Herrmann *et al. Bull. Am. Phys. Soc.*, vol. 41, p. 1381, 1996.

[59] J. D. Strachan *et al. Rev. Sci. Instrum.*, vol. 66, p. 1247, 1995.

[60] E. Fredrickson *et al. Rev. Sci. Instrum.*, vol. 57, p. 2084, 1986.

[61] A. Janos *et al. Rev. Sci. Instrum.*, vol. 66, p. 668, 1995.

[62] Z. Chang *et al. Phys. Rev. Lett.*, vol. 76, p. 1071, 1996.